Journal of
Micro/Nanolithography,
MEMS, and MOEMS

Nanolithography.SPIEDigitalLibrary.org

High-voltage CD-SEM-based application to monitor 3D profile of high-aspect-ratio features

Wei Sun
Hiroya Ohta
Taku Ninomiya
Yasunori Goto

SPIE.

Wei Sun, Hiroya Ohta, Taku Ninomiya, Yasunori Goto, "High-voltage CD-SEM-based application to monitor 3D profile of high-aspect-ratio features," *J. Micro/Nanolith. MEMS MOEMS* **19**(2), 024002 (2020), doi: 10.1117/1.JMM.19.2.024002

High-voltage CD-SEM-based application to monitor 3D profile of high-aspect-ratio features

Wei Sun,[a,*] Hiroya Ohta,[b] Taku Ninomiya,[b] and Yasunori Goto[b]
[a]Hitachi, Ltd., Research & Development Group, Tokyo, Japan
[b]Hitachi High-Tech Corporation, Ibaraki, Japan

Abstract

Background: In-line metrology for three-dimensional (3D) profiling high-aspect-ratio (HAR) features is highly important for manufacturing semiconductor devices, particularly for memory devices, such as 3D NAND and DRAM.

Aim: Our purpose was to obtain the cross-sectional profiles of the HAR features from top-view critical dimension scanning electron microscopy (CD-SEM) images.

Approach: Based on Monte Carlo simulation results, we proposed a method for 3D profiling of HAR features using backscattered electron (BSE) signal intensities. Several kinds of HAR holes with different taper angles and bowing geometries were fabricated. High-voltage CD-SEM was used for experiments to determine the feasibility of our approach.

Results: Using the BSE line-profile, we constructed cross sections of the taper holes and estimated sidewall angles (SWAs), which were approximately the same as those observed using field-emission scanning electron microscopy (FE-SEM). The constructed cross sections of the bowing holes and the trends of the geometric variance, which were estimated by the middle CD and its depth, were consistent with the cross sections observed by FE-SEM.

Conclusions: The results demonstrate that the variation in the HAR holes, such as SWA and bowing geometry, can be measured and monitored using the BSE images.

 [DOI: 10.1117/1.JMM.19.2.024002]

Keywords: critical dimension scanning electron microscopy; three-dimensional metrology; in-line; backscattered electrons; high-aspect-ratio; high voltage.

Paper 19104 received Dec. 20, 2019; accepted for publication Apr. 28, 2020; published online May 12, 2020.

1 Introduction

Semiconductor devices are becoming highly integrated by shrinking dimensions. However, the limitation of scaling down drives the devices from planar to complicated three-dimensional (3D) structures, such as 3D NAND.[1] One of the features of the 3D NAND is high-aspect-ratio (HAR) channel holes, having a top diameter of about 100 nm and a depth of several micrometers. The aspect ratio, which is defined as the ratio of the depth to the top diameter of the channel holes, has increased to 50:1 and beyond.[2] Increasing the aspect ratio makes it more challenging to prevent distortion from the top to the bottom during etching. Moreover, more than a trillion holes must be etched simultaneously and uniformly on each wafer in high-volume manufacturing (HVM).[2] As shown in Fig. 1, the etched HAR holes appear to have various geometries, such as tilting, bowing, and twisting. As irregular and curvature channel holes cause fatal problems in device performance, significant efforts in process control and metrology are required in HVM. Therefore, an in-line metrology for measuring the typical features of the HAR holes is becoming more challenging and crucial for yielding improvement. Except for measuring the bottom critical dimension (CD) and overlay between the top center and the bottom center, demand has been

*Address all correspondence to Wei Sun, E-mail: wei.sun.pt@hitachi.com

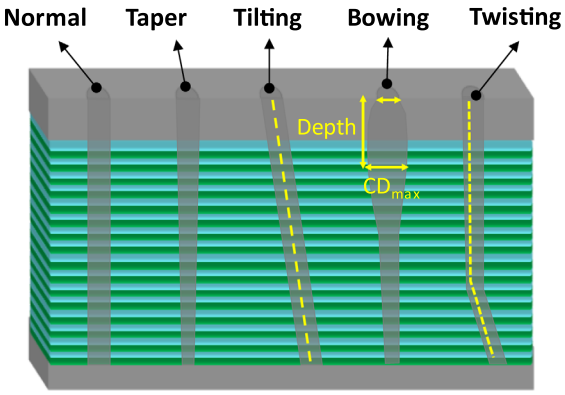

Fig. 1 Various possible geometries of the HAR holes after the etching process.

increasing for in-line measurements of the cross-sectional profile or 3D profile of the HAR holes with complicated geometries, such as bowing and twisting.[2,3]

So far, many technologies have been explored to enable the in-line 3D metrology for the HAR holes, including both spectroscopic-based techniques and scanning electron microscopy (SEM)-based imaging techniques. Optical scatterometry [so-called optical critical dimension (OCD)] and critical dimension small angle x-ray spectroscopy (CD-SAXS) have been investigated.[4,5] OCD is a model-based nondestructive in-line metrology technique that is fast and capable of measuring structural variations, such as the CD and profile across the wafer. However, it often has difficulties in material optimization and high correlation between material parameters and complex geometries. CD-SAXS is a new variable-angle transmission scattering technique that has been shown to be capable of characterizing 3D shapes of periodic nanostructures. A commercial solution is not available yet due to the lack of an adequate high brightness source.[5–7] Another optical method is through-focus scanning optical microscopy, which can identify process variations across the wafer. However, it may be hard to distinguish purely CD and sidewall angle (SWA) differences.[8]

For SEM-based imaging techniques, one of the issues arising from the HAR holes is the extremely small opening solid angle, which prevents the secondary electrons (SEs) from escaping from the bottom of the holes. Therefore, the prerequisite condition for measuring the bottom CD and the 3D profiles of the HAR holes is detecting the signals emitted from the bottom of the holes. Aron et al.[9] investigated environmental SEM and high-voltage SEM operated at 15 kV to detect the SEs and the electrons that are generated by the backscattered electrons (BSEs). However, the bottom of the holes could not be imaged successfully because of the issues of the charging effect and the insufficient bottom information provided by SEs.

As for the aforementioned limitations, in-line 3D metrology methods are still being developed to enable distinguishing the relative variation not only in the geometry but also in the absolute 3D profile of individual and periodic HAR features. We previously demonstrated that using high acceleration voltage and detecting the BSEs, with solid angles larger than 0.002π sr and energies higher than 1 keV, are effective ways to obtain the signals emitted from the bottom of the HAR holes. Moreover, Monte Carlo simulation results showed that the relationship between the BSE signal intensity emitted from the HAR holes and the depth of the irradiation location can be mathematically represented by an exponential function. The approach computed the depth from the BSE signal intensity, which allows for construction of the cross-sectional profile from the BSE line-profiles.[10]

Experiments were performed to determine the feasibility of the proposed method. Several kinds of HAR holes with different taper angles and different bowing geometries were fabricated for evaluation. The cross-sectional profiles constructed using the BSE line-profiles were compared with the cross sections that were observed using a field-emission scanning electron microscopy (FE-SEM). The results show that the geometric variation in the HAR holes, such as SWA and bowing, can be measured and monitored using the BSE images obtained by the high-voltage critical dimension scanning electron microscopy (HV-SEM).

2 Methods

2.1 *Mathematical Model*

When the electron beam (EB) passes through a material, electrons experience elastic and inelastic scattering or pass through without being scattered. The longer the travel path in the material, the more scattering events electrons experience, causing the electron to lose energy. Consequently, the number of electrons decreases. The decrease in EB intensity can be modeled as a function of the depth traversed in the material[11–13] using the Beer–Lambert law.[14]

The decrease in the beam intensity can be described as

$$I(h) = I_0 \exp(-\mu_0 h), \tag{1}$$

where I_0 is the intensity of the incident EB, $I(h)$ is the intensity of the EB after traveling through depth h in the material, and μ_0 is the attenuation coefficient of the material.

Therefore, we were motivated to estimate the depth information from the signal intensity in the BSE image. In previous work, we investigated the relationship between the BSE signal intensity and the depth in the holes through a Monte Carlo simulator of Chariot (aBeam Technologies). As shown in Fig. 2,[10] electrons with energy ranging from 30 to 45 keV were irradiated into one of the HAR holes being periodically etched in the material. The top CD was 100 nm while the depth from the top to the bottom of the HAR hole (H) ranged from 3 to 7 μm. An annular detector was configured to collect these BSEs with solid angles larger than 0.002π sr and energies higher than 1 keV. The cavity volume for the HAR holes is typically from 10% to 30% of the interaction volume of the material. In addition, electrons with solid angles smaller than 0.002π sr, enabling escape through the openings of the HAR holes, accounted for only a very small fraction of the total BSEs (<2%). Under these specified conditions, the simulation results show that the BSE signal intensities emitted from the irradiation location along the sidewall of the HAR holes can be approximately represented by Eq. (1). Thus, the BSE signal intensity emitted from depth (h) relative to the intensity at the top surface ($h = 0$) can be represented by

$$\mathrm{BSE}(h)/\mathrm{BSE}(0) = e^{-\mu h}, \tag{2}$$

where h is the depth from the specimen surface to the irradiation location and μ is the attenuation coefficient, which determines how fast the signal intensity decreases with the depth.

Equation (2) provides a convenient method to correlate the relative BSE signals intensities with the depth of the HAR holes. We also found that μ depends on the energy of the incident

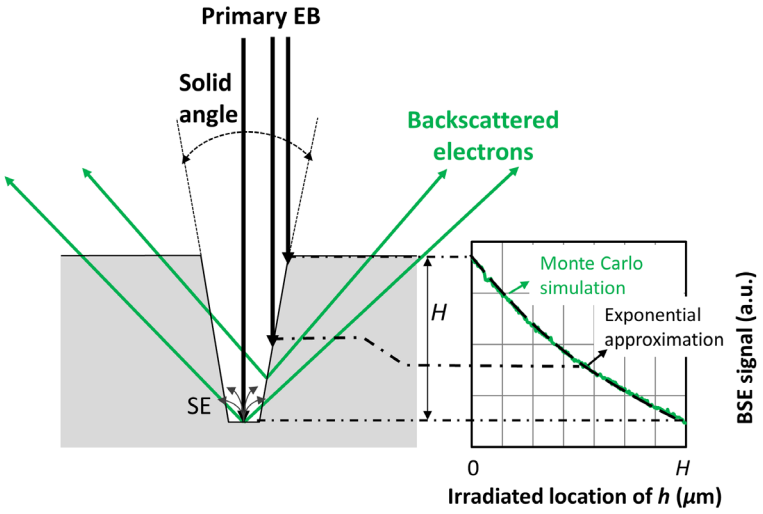

Fig. 2 Schematic of the irradiation of the primary EB on the top, the middle sidewall, and the bottom of an HAR hole. When detecting the electrons with solid angles larger than the opening solid angle of the HAR hole, the correlation between the BSE signal intensity and the irradiation location along the sidewall can be approximately represented by an exponential function.

electrons and on the depth and pattern density of the HAR holes, but it is independent of the extremely small variation in the SWA or the tilt angle of the primary EB. Some cases having the same value of μ are applicable to HAR holes with different depths when using a high-energy EB.[10]

However, it is necessary to address the BSE signal intensity failing to follow the exponential law when the opening solid angle or the cavity volume of the holes becomes large so that the electrons escaping from the openings of the holes represent a large fraction of the total BSEs. Fortunately, we found that the applicable range of Eq. (2) covers the measurement target HAR holes (etched in Si and SiN/SiO_2 stacked layers) with an aspect ratio higher than 15.

2.2 *Profiling the Cross Section of HAR Holes*

The reconstruction of the cross section using the BSE images can be obtained by the following procedures.

1. The BSE line-profile from a BSE image is acquired in the direction in which the cross section is expected to be measured (e.g., in the x direction). Typically, the contrast in SEM images only represents the variation in the signal intensity. We know that the bright area in the BSE image of the HAR holes corresponds to the top, while the dark area corresponds to the bottom. However, the depth from the top to the bottom of the HAR hole is not included in the BSE image. For unification and convenience, the BSE signal intensity represented by the grayscale is normalized as

$$\mathrm{BSE}(h) = (e^{-\mu h} - e^{-\mu H})/(e^{-0} - e^{-\mu H}), \qquad h = (0, H), \tag{3}$$

   where 0 and H denote the top surface and the depth from top to bottom, respectively, and μ is the coefficient that determines how fast the signal intensity decreases with the depth. The BSE signal intensity at the top is set to 1 while the signal intensity at the bottom ($h = H$) is set to 0 (0%). Unlike the SE image, there is no signal peak in the BSE image for searching the top edge of the hole. The BSE signal intensity for detecting the two top edges can be determined from the width between those two edges, which is the CD being measured in-line using the SE image.
2. According to the relationship between the signal intensity and the depth, h can be calculated as follows:

$$h = -\ln[\mathrm{BSE}(h)(1 - e{-^{\mu H}}) + e{-^{\mu H}}]/\mu. \tag{4}$$

   Here it is necessary to know the values of μ and H in advance. H can be estimated from the cross section or the etching process. When we consider the EB having infinitively small spot size and aperture angle, the value of μ can be obtained by calibrating the constructed cross-sectional profile against its cross-sectional geometry. If the cross-sectional geometry of the target for calibration is unavailable, μ can be derived by fitting the Monte Carlo simulated BSE signal emitted from the target HAR holes. The simulation needs to be performed on the specified measurement target and the detection configuration. In this work, μ was derived by fitting the simulated BSE signal intensities, which were calculated in accordance with the specification of the fabricated specimen and the detection configuration of the HV-SEM. Thus, the cross-sectional profile can be created by plotting h against the x coordinate with a suitable origin point (e.g., by selecting the top center of the hole as the origin point).
3. When measuring the HAR holes with bowing geometry, we need to tilt the EB positively and negatively to observe the left and the right sidewalls, respectively. After calculating the depth, a process of coordinate transformation is performed according to the tilt angle to derive the cross-sectional profile in the perpendicular coordinates when using a tilt observation. Finally, the cross-sectional profile of a bowing hole can be reconstructed by combining two halves of the profiles that are observed by negative tilt for the left sidewall and positive tilt for the right sidewall.

2.3 *HAR Hole Samples*

Several kinds of HAR holes (aspect ratio > 13) with different taper angles and bowing geometries were etched in different silicon wafers to determine the feasibility of the algorithm. The ratio of SF_6/O_2 gas and the etching time were tuned to vary the cross-sectional profile of the HAR holes. The top CD was around 300 nm, and the pitch was 600 nm. The center coordinates of a group of the HAR holes were shifted by 10 nm in the x direction so that different cross-sectional planes along the x direction can be obtained by cleaving the wafer. The cross-sectional plane with the largest top CD was selected and considered as the one bisecting the hole. The as-cleaved cross sections of each specimen were observed using an FE-SEM (Hitachi, S-4800). As the SEM images shown in Fig. 3, the depths of the taper-etched holes (specimens 1 to 3) and the bowing-etched holes (specimens 4 to 6) were 3.5 and 4 μm, respectively.

We used Terminal PC Offline CD Measurement Software to measure the CD located at different depths from the observed cross sections. The depth was measured from the top surface to a specified position, while the CD at this depth was determined by the distance between the left and right edge positions, which were distinguished from the maximum of the gray level. The CDs of eight of the holes in each FE-SEM image were measured, and the average values were calculated. When the shape of the taper holes approximated a symmetric trapezoid, the SWA was calculated by taking the arctangent of the half CD difference divided by the depth. Table 1 shows the measured CDs at the top and at the depth of 3 μm and the estimated SWA of each specimen. Table 2 shows the measured CDs at the top, the middle CD (MCD), and the depth of MCD for the bowing holes. The maximum standard deviation of the measured CDs by sampling the eight holes in the FE-SEM images was ± 13 nm, corresponding to ± 4 pixels in the FE-SEM images.

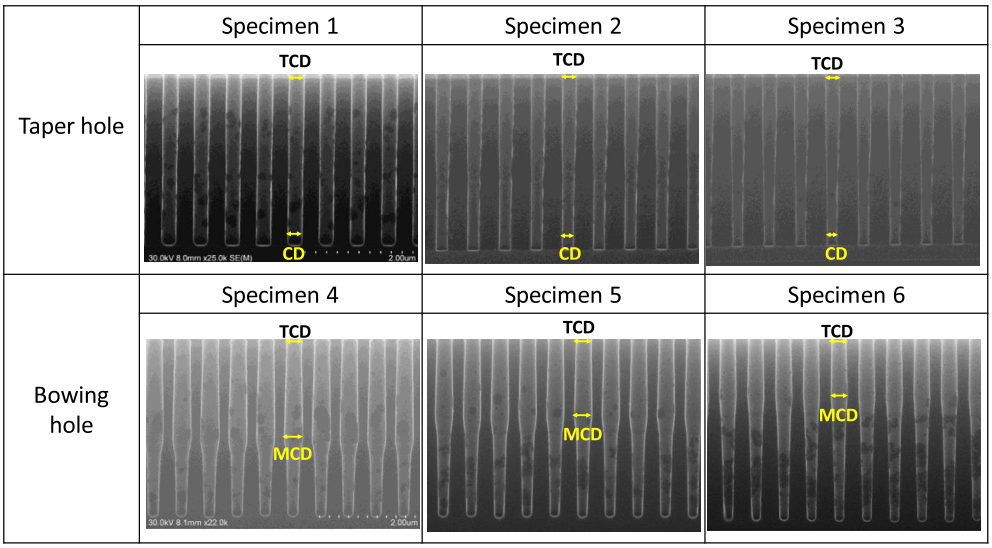

Fig. 3 FE-SEM images of the as-cleaved cross sections of the taper and bowing HAR holes.

Table 1 The measured CDs at the top and at the depth of 3 μm and the estimated SWAs of the taper holes from the observed cross sections.

	Specimen number		
	1	2	3
CD at top (nm)	268 ± 7	240 ± 13	232 ± 13
CD at 3 μm (nm)	250 ± 10	194 ± 10	165 ± 13
SWA (deg)	0.17 ± 0.16	0.44 ± 0.22	0.64 ± 0.25

Table 2 The measured CDs at the top, the MCD, and MCD depth of the bowing holes from the observed cross sections.

	Specimen number		
	4	5	6
CD at top (nm)	269 ± 13	278 ± 7	288 ± 10
MCD (nm)	338 ± 10	317 ± 7	297 ± 7
Depth of MCD (nm)	2300	1800	1300

As a result, the estimated SWAs had a deviation from ± 0.16 deg to ± 0.25 deg. However, the top CD and bottom CD, which were measured using the SE and BSE images of the HV-SEM, respectively, had a very small deviation of ± 1.7 nm among eight of holes. The HV-SEM measurement results indicate that the hole-to-hole geometric variation was very small. The large uncertainty of the CDs and the SWAs in Tables 1 and 2 can be attributed to the variance of the distinguished edge positions, which were easily affected by the grayscale of the sidewall edge in the FE-SEM images. In addition, it is noteworthy that the measured values of the specimens may have had experimental errors, which were generated during the sampling and observation of the as-cleaved cross sections using the FE-SEM.

The SWA of the taper holes, the MCD, and its depth of the bowing holes measured from the observed cross sections will be taken as a reference and compared with the results that were measured from the constructed cross-sectional profiles.

2.4 *HV-SEM Observation and BSE Image Analysis*

Because the hole-to-hole geometric variation was small, the HAR holes near those observed using FE-SEM were selected and observed using the HV-SEM (Hitachi, CV5000). Figure 4 shows the BSE images obtained using an acceleration voltage of 30 kV and a long depth of field (DOF). The spot size and the aperture angle of the primary EB in the experiments were supposed to be a few nanometers and several milliradians. The BSE images were obtained using the following conditions. The number of frame integrations was 32. Because the measurement

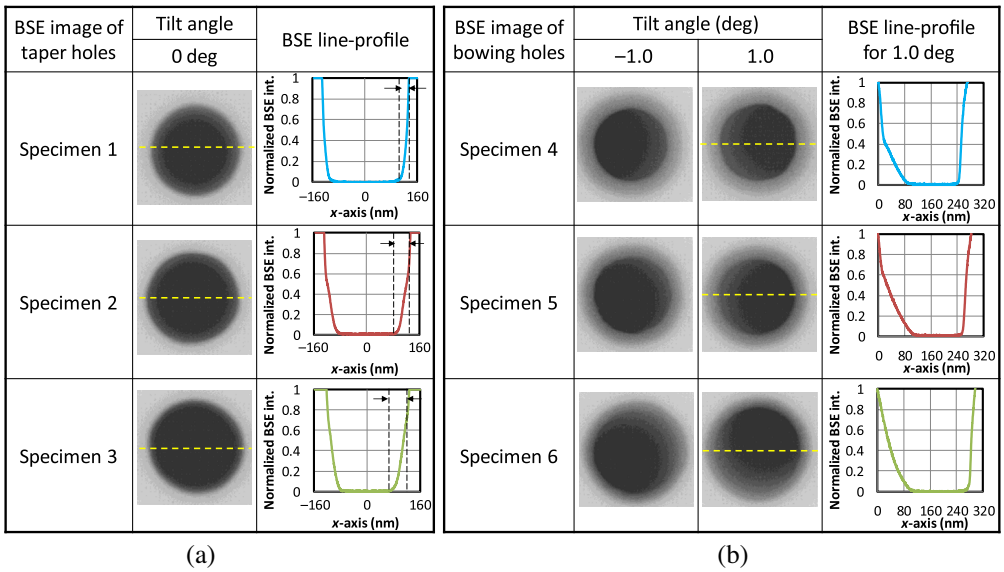

Fig. 4 BSE images obtained using the high-voltage CD-SEM at 30 kV with the DOF mode and their normalized line-profiles taken through the center of the HAR holes. The tilt angle of the primary EB was (a) 0 deg for the taper holes and (b) ± 1 deg for the bowing holes.

accuracy in the depth direction was significantly affected by the pixel size of the images when observing the approximately vertical sidewall, the BSE images had a field-of-view as small as 385 nm and the pixel size was 0.376 nm.

From the bowing holes (specimens 4 to 6) shown in Fig. 3, it is observed that the primary EB with an incident angle of 0 deg (perpendicular to the wafer) could not irradiate on the region of the reverse taper. The tilt angle of the primary EB was changed according to the geometry of the HAR holes. The tilt angle of the EB was 0 deg when observing the taper holes. Figure 4(a) shows the BSE images of taper holes (specimens 1 to 3) and its normalized BSE line-profile taken through the center of the holes, as displayed by the dashed line. By observing the BSE line-profiles, we see that the slope width in the profile increased as the SWA of the hole increased, as shown by the arrows. Figure 4(b) shows BSE images of the bowing holes (specimens 4 to 6). The primary was tilted by 1 deg and -1 deg along the x axis, respectively, to observe the reverse taper at the left and right sides of the bowing holes, respectively. It is noteworthy that the tilt angle of the primary EB was greater than the angles of the reverse taper of these three specimens to make sure that the sidewall could be irradiated. From the BSE line-profiles for 1 deg taken through the center of the holes, we observe that the contrast corresponding to the left sidewall of the bowing holes appeared in the direction in which the primary EB was tilted. This indicates that the sidewall of the bowing holes can be seen using the tilted EB.

3 Results and Discussions

3.1 *Cross-Sectional Profiles of the Taper HAR Holes*

In Fig. 5(a), the experimental BSE line-profiles taken from the BSE images (at a tilt angle of 0 deg) of the taper holes (specimens 1 to 3) are displayed together. Each line-profile was normalized by the signal difference between the bottom surface and the top edge. The depth h was calculated from the normalized BSE signal intensity, as shown in Fig. 5(a) using Eq. (4). Here,

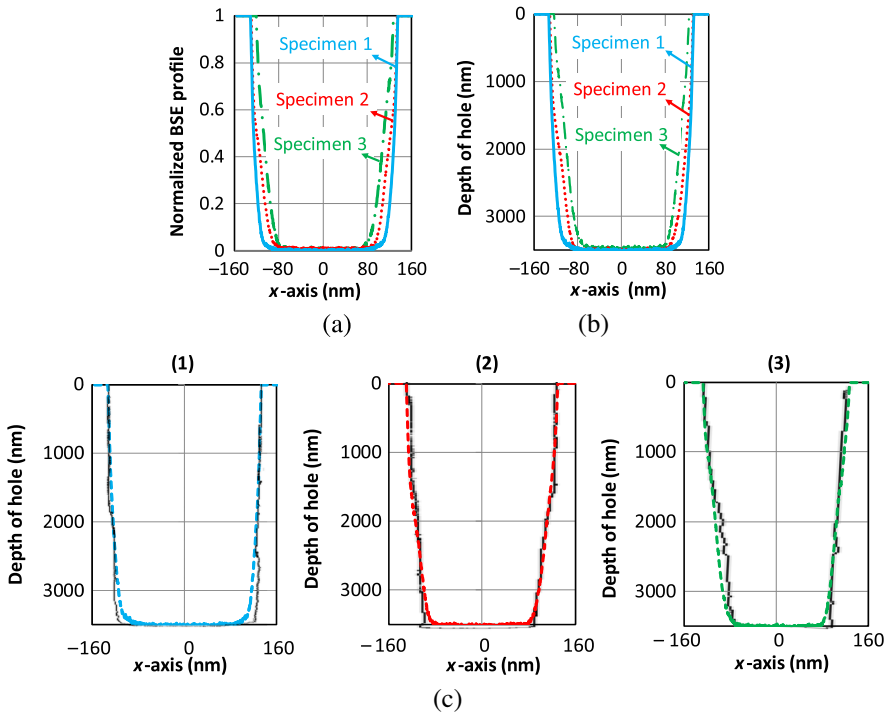

Fig. 5 (a) Normalized BSE line-profiles of the taper holes with SWAs at a tilt angle of 0 deg. (b) Constructed cross-sectional profile of the taper holes using the BSE line-profiles shown in (a). (c) Comparison of the constructed cross-sectional profiles (dashed line) of specimens 1 to 3 with the extracted cross sections (solid line) from the FE-SEM images.

Table 3 The measured CDs at the top and at the depth at 3 μm and the estimated SWAs of the taper holes using the constructed cross-sectional profiles.

	Specimen number		
	1	2	3
CD at top (nm)	262	256	246
CD at 3 μm (nm)	231	208	181
SWA (deg)	0.30	0.46	0.62

the coefficient $\mu = 0.13\ \mu\text{m}^{-1}$ was obtained by fitting Monte Carlo simulated BSE signal intensities, and the depth of the taper holes was measured from the observed cross sections. Figure 5(b) shows the constructed cross-sectional profiles by plotting the depth of the holes against the x coordinate with the origin point at the top center of the holes. To compare the constructed cross-sectional profiles with the observed cross sections, the sidewall edges of the holes were extracted from the FE-SEM image using ImageJ software. In Fig. 5(c), the constructed cross-sectional profile of each taper hole (specimens 1 to 3) is plotted together with the cross section extracted from the FE-SEM image. Without considering the roughness caused by the binary processing during the edge extraction, we observe that the constructed cross-sectional profiles were approximately consistent with the observed cross sections. Some discrepancies can be seen near the bottom edges of the taper holes between each pair of the cross sections, especially for specimen 1.

Table 3 shows the CDs at the top and at the depth of 3 μm and the estimated SWAs of the taper holes, which were measured from the constructed cross-sectional profiles. The SWAs calculated from the constructed cross-sectional profiles were 0.30, 0.46, and 0.62 deg, respectively. Comparing Tables 1 and 3, the trends of CD decreasing and SWA increasing were inconsistent. Although differences occurred in the measured CDs between these two methods, most of the measured CD values in Table 3 were close to the range of values in Table 1. One exception was the small CD value of 231 nm at 3 μm for specimen 1, resulting in a relatively large SWA. The reasons for this will be discussed later. These results show that the SWA difference can be distinguished and measured quantitatively from the constructed cross-sectional profiles.

3.2 *Cross-Sectional Profiles of the Bowing HAR Holes*

In Fig. 6(a), examples of the normalized experimental BSE line-profiles (at a tilt angle of 1 deg) of the bowing holes are plotted together. When the left side of the sidewall was irradiated by a 1 deg tilted primary EB, we see that the profile had an inflection point on the left side. The shape differences in the BSE line-profiles and the location differences in the inflection point reflect the geometric differences of the bowing holes. Figure 6(b) shows the constructed cross-sectional profiles of the bowing holes. As with the method described earlier, the cross-sectional profiles connected two halves of the profiles, which were reconstructed using the BSE line-profiles by 1 and -1 deg for the left sidewall and the right sidewall, respectively. In Fig. 6(c), the constructed cross-sectional profile of each bowing hole (specimens 4 to 6) is plotted together with the cross section extracted from the FE-SEM images. Compared to the extracted cross sections, the constructed cross sections of the bowing holes smoothed out and the bottom edges became a little rounded. Although the cross-sectional profiles were not completely the same, the bowing shape and the geometric differences among the three specimens could be distinguished.

Table 4 shows the CDs at the top, the MCD, and the MCD depth for the bowing holes, which were measured from the constructed cross-sectional profiles in Fig. 6(c). The measured MCD and its depth of specimens 4 to 6 were 316 nm at 1900 nm, 308 nm at 1400 nm, and 304 nm at 700 nm, respectively. Similar to the results of the taper holes, although the measured MCD and its depth had differences between the values shown in Tables 2 and 4, the trends of MCD and MCD depth decrease from specimens 4 to 6 were in good agreement. Except for the MCD value

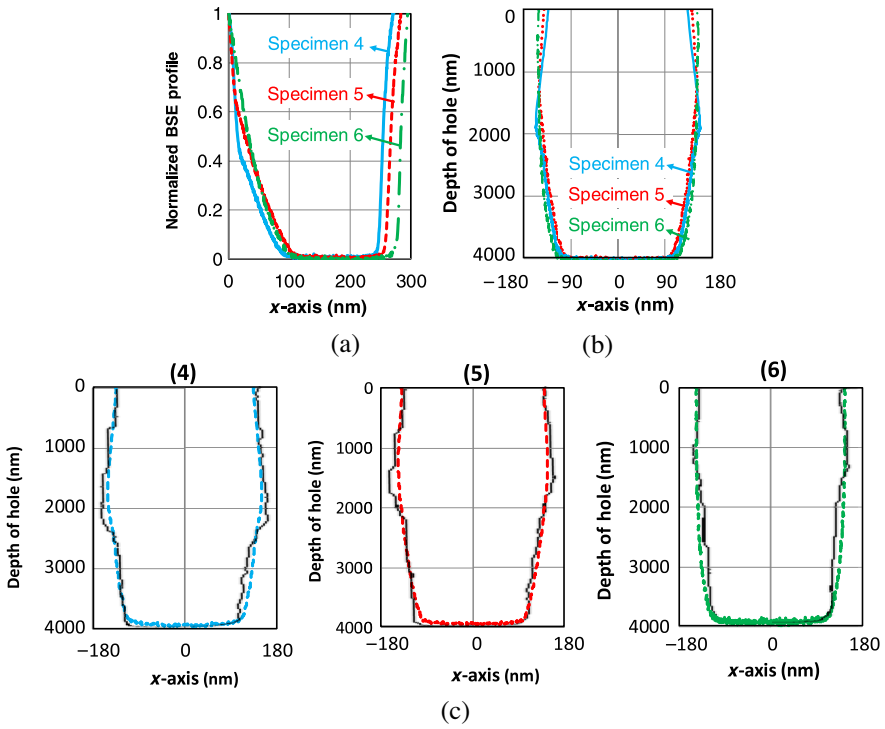

Fig. 6 (a) Normalized BSE line-profiles of the holes with different bowing shapes at a tilt angle of 1 deg. (b) Constructed cross-sectional profile of the bowing holes using the BSE line-profiles obtained at ±1 deg. (c) Comparison of the constructed cross-sectional profiles (dashed line) of specimens 4 to 6 with the extracted cross sections from the FE-SEM images (solid line).

Table 4 The measured CDs at the top, the MCD, and MCD depth of the bowing holes using the constructed cross-sectional profiles.

	Specimen number		
	4	5	6
CD at top (nm)	268	281	299
MCD (nm)	316	308	304
Depth of MCD (nm)	1900	1400	700

of specimen 4, most of the MCD values in Table 4 were close to the range of values in Table 2. By contrast, all of the values of the MCD depth in Table 4 were smaller than those in Table 2, which can be attributed to the fact that the sharply curved bottom edges and the bowing curvature get smoothed out due to the blurring of the EB.

The BSE signal intensity was supposed to follow the exponential law at the condition of the primary EB having an infinitively small spot size and aperture angle (so-called point beam). However, the BSE images were obtained by scanning an EB in an SEM. The primary EB in the SEM was not a point beam but had spot size of several nanometers and an aperture angle of a few milliradians, which was determined by the optical design. As a result, a kind of blurring occurred. The BSE line-profile must have small deviations from the ideal exponential function, which in turn induced errors in the constructed cross-sectional profile. As shown in Figs. 5(c) and 6(c), the sharply varied bottom edge and the bowing geometry in the constructed cross sections became round, resulting in larger differences in the measured SWA (specimen 1) and the bowing features (specimen 4) than the others. Theoretically, it is possible to calibrate μ by

taking into account the effect the spot size and the aperture angle when we know the cross section of the measurement target. In this case, μ is not a constant value but is dependent on the sidewall geometry of the hole and the tilt angle of the EB. However, when we measure a new target hole with unknown geometry, we encounter an intractable problem in which calibrating μ according to its geometry requires using the calibrated μ. Instead of solving this problem by mathematics, we applied the learning approach to improve the profiling accuracy by considering the effect of the spot size and the aperture angle.[15]

To determine the feasibility of the approach, the bowing holes were fabricated and observed using a pair of tilt images (± 1 deg). When the sidewall of the HAR holes can be irradiated directly by the primary EB, the cross section can be reconstructed using a series of BSE images taken at different tilt angles. However, when the angle of the reverse taper is over the tilt range of the primary EB or the primary EB is cut off by the opposite top edge before it arrives at the sidewall of the hole, the geometry of the reverse taper could not be obtained correctly. By contrast, when keeping the width dimension constant and increasing the depth of the holes, it is necessary to increase the energy of the primary EB to enable the electrons to penetrate from the bottom of the hole through the top surface of the material. The necessary electron energy can be estimated using Monte Carlo simulation according to the depth of the observation target. Further experimental evaluations will be performed on the HAR holes with more complicated geometries and a higher aspect ratio.

4 Conclusions and Outlook

We demonstrated an application to identify and monitor the geometric variation of HAR holes using BSE signal intensities. This method correlates the BSE signals intensity and the depth in the HAR holes using an exponential function, which is valid when detecting those BSEs with solid angles larger the small opening solid angle of the HAR holes. This correlation allows for calculating the depth from the BSE signal intensity and constructing a cross-sectional profile of the HAR hole. Several kinds of HAR holes with different taper angles and bowing shapes were fabricated for an experimental evaluation. The BSE images were obtained using high-voltage CD-SEM with an acceleration voltage of 30 kV. Using the BSE line-profiles, we constructed cross sections of the taper holes and the bowing holes. Although the bottom edge and the bowing curvature in the constructed cross-sectional profiles became smoothed out and rounded due to the spot size and the aperture angle of the EB, the estimated geometric variation in the SWA, MCD, and its depth were consistent with those measured from the observed cross sections. The measurement results suggest that geometric variation in HAR holes can be quantitatively estimated from the constructed cross sections. This approach facilitates in-line monitoring of the process-induced geometric variation in the HAR holes using high-voltage CD-SEM.

Acknowledgments

We would like to thank Makoto Sakakibara of the R&D Group of Hitachi, Ltd. for his many insightful opinions on the simulation studies and CD metrology in general. We would like to thank Jiro Yamamoto, Toshiyuki Mine, and the members concerned in the Energy Conversion Electronics Research Department of R&D Group of Hitachi, Ltd. for their support in the specimen fabrication. We are also grateful to Makoto Suzuki Hitachi High-Technologies for their support during the simulations.

References

1. IEEE Rebooting Compute, "The international roadmap for devices and systems (IRDS): 2017 edition," 2018, https://irds.ieee.org/images/files/pdf/2017/2017IRDS_MET.pdf.
2. H. Xiao, *3D IC Devices, Technologies, and Manufacturing*, SPIE Press, Bellingham, Washington (2016).
3. P. Christopher, "3D memory: etch is the new litho," *Proc. SPIE* **10589**, 1058904 (2018).

4. C. Settens et al., "Critical dimension small angle x-ray scattering measurements of FinFET and 3D memory structures," *Proc. SPIE* **8681**, 86810L (2013).
5. D. Sunday et al., "Determination of the internal morphology of nanostructures patterned by directed self-assembly," *ACS Nano* **8**, 8426–8437 (2014).
6. D. F. Sunday et al., "Determining the shape and periodicity of nanostructures using small-angle x-ray scattering," *J. Appl. Cryst.* **48**, 1355–1363 (2015).
7. Y. Ito et al., "Characterization of cross-sectional profile of resist L/S and hole pattern using CD-SAXS," *Proc. SPIE* **9778**, 97780L (2016).
8. K. A. Ravi et al., "Feasibility study on 3-D shape analysis of high-aspect-ratio features using through-focus scanning optical microscopy," *Opt. Express* **24**(15), 16574–16585 (2016).
9. J. C. Aron et al., "Scanning electron microscopy imaging of ultra-high aspect ratio hole features," *Proc. SPIE* **8324**, 83241N (2012).
10. S. Wei et al., "Depth-correlated backscattered electron signal intensity for 3D-profile measurement of high aspect ratio holes," *Microscopy* **68**, 385–394 (2019).
11. P. J. Goodhew et al., *Electron Microscopy and Analysis*, 3rd ed., pp. 31–35, CRC Press, London, New York (2001).
12. Z. Huairuo et al., "Local thickness measurement through scattering contrast and electron energy-loss spectroscopy," *Micron* **43**, 8–15 (2013).
13. S. V. Venkatakrishnan et al., "Model based iterative reconstruction for bright field electron tomography," *IEEE Trans. Comput. Imaging* **1**, 1–15 (2015).
14. E. Zeitler et al., "Contributions to quantitative electron microscopy," *J. Appl. Phys.* **30**, 940–944 (1959).
15. S. Wei et al., "Accuracy improvement of 3D-profiling for HAR features using deep learning," *Proc. SPIE* **11325**, 113250N (2020).

Wei Sun is a researcher at the Center for Technology Innovation, Research & Development Group, Hitachi, Ltd. She received her BS and MS degrees in materials from Xi'an JiaoTong University and her PhD in electrical and electronics engineering from Kyushu University in 2011. Her current research interests include electron beam microscopy and metrology for advanced semiconductor devices.

Hiroya Ohta received his master's degree in electrical engineering from Keio University, Japan. He joined Hitachi Ltd. (Hitachi High-Tech Corporation) in 1990 and is currently engaged in the development of electron beam optics in SEM for semiconductor inspection and metrology.

Taku Ninomiya received his bachelor's degree in Faculty of Science and Technology, Department of Physics from Tokyo University of Science, Japan. He joined Hitachi Ltd. (Hitachi High-Tech Corporation) in 1988 and is currently engaged in the development of CD-SEM for semiconductor inspection and metrology.

Yasunori Goto received his master's degree in Faculty of Engineering from Kyusyu University, Japan. He joined Hitachi High-Tech Corporation in 1998 and is currently engaged in the development of CD-SEM for semiconductor inspection and metrology.